

Collapse of Primordial Clouds

Sandra R. Oliveira, Oswaldo D. Miranda, José C. N. de Araujo
and Reuven Opher

*Instituto Astronômico e Geofísico – Universidade de São Paulo
Av. Miguel Stéfano 4200, São Paulo, 04301-904, SP, Brazil*

ABSTRACT

We present here studies of collapse of purely baryonic Population III objects with masses ranging from $10M_{\odot}$ to 10^6M_{\odot} . A spherical Lagrangian hydrodynamic code has been written to study the formation and evolution of the primordial clouds, from the beginning of the recombination era ($z_{rec} \sim 1500$) until the redshift when the collapse occurs. All the relevant processes are included in the calculations, as well as, the expansion of the Universe. As initial condition we take different values for the Hubble constant and for the baryonic density parameter (considering however a purely baryonic Universe), as well as different density perturbation spectra, in order to see their influence on the behavior of the Population III objects evolution. We find, for example, that the first mass that collapses is $8.5 \times 10^4 M_{\odot}$ for $h = 1$, $\Omega = 0.1$ and $\delta_i = \delta\rho/\rho = (M/M_o)^{-1/3}(1+z_{rec})^{-1}$ with the mass scale $M_o = 10^{15}M_{\odot}$. For $M_o = 4 \times 10^{17}M_{\odot}$ we obtain $4.4 \times 10^4 M_{\odot}$ for the first mass that collapses. The cooling-heating and photon drag processes have a key role in the collapse of the clouds and in their thermal history. Our results show, for example, that when we disregard the Compton cooling-heating, the collapse of the objects with masses $> 8.5 \times 10^4 M_{\odot}$ occurs earlier. On the other hand, disregarding the photon drag process, the collapse occurs at a higher redshift.

Key words: Cosmology: theory – early Universe.

1 INTRODUCTION

The formation of galaxies, or pre-galactic objects, in the early Universe is one of the most important fields of study in cosmology. It is not completely known, however, how the various structures observed have been formed. It is not completely clear how the density perturbations, that are the seeds for the formation of the structures of the Universe, were produced and how they evolved to produce the structures that we observe.

Some authors argued that for scales below $0.1Mpc$ the purely gravitational simulations are not completely appropriate, due to the fact that non-gravitational physical processes are preponderant (Cen 1992). Thus, the more convenient manner of studying these scales is to use a hydrodynamic code and to include all the physical processes that are important during and after the recombination era, starting the calculations from the beginning of the recombination era. As it will be shown in the present paper, we make such a study.

Studies including the cooling-heating processes of the gas, in particular of pre-galactic composition, have been considered since the 1960's (e.g., Matsuda et al 1969, Hutchins et al 1976, Calberg 1981, Palla et al 1983 among others). These articles consider pressure free gas clouds collapsing and analyzed the effects of the physical processes. Recently,

some authors considered the pressure of the gas among other physical processes in the gas dynamics (de Araujo 1990, de Araujo & Opher 1988, 1989, 1994, Haiman et al 1995, Thoul & Weinberg 1995 among others).

For example, de Araujo & Opher (1988) studied the collapse of primordial clouds using an isothermal density perturbation spectrum. They included the internal pressure, the influence of the cosmic background radiation and several cooling-heating processes; among them are: photon cooling, photon drag, photoionization due to the CBR, collisional ionization and a set of equations for the creation and destruction of H_2 molecules, as well as the expansion of the Universe. All these processes are present during and after the recombination era, therefore, they are essential to be taken into account.

In particular, de Araujo & Opher (1989) used a complete set of hydrodynamic equations and assumed that the density contrast profile is uniform (“top hat” like) throughout the calculation. Thus, the resulting system of equations is dependent only on time. As a consequence, the velocity profile is linear in the spherical radial coordinate. This approximation could be good but a detailed analysis shows that the physical parameters can change their values for different points inside the cloud, as we are showing in the present work. Also, it is not realistic to consider that the cloud, as a whole, will collapse; a possible partial collapse is

more realistic.

In the present article we used the same set of hydrodynamic equations of de Araujo & Opher (1988). We rewrote it to use a spherical Lagrangian hydrodynamic code to follow the variables of the fluid. We analyzed the internal structure of the cloud during the collapse, using the same spectrum of density perturbations used by de Araujo & Opher (1988), to verify the differences in the behavior of the physical parameters when we include the internal morphology.

The spherical Lagrangian hydrodynamic code (written by one of us, ODM) divides the cloud in several concentric shells. This number of shells is the optimal combination for the variable time step and the number of shells that gives the shortest processing time. Our results show that 450 shells are enough to model satisfactorily all the clouds here studied. To verify if the number of shells is an optimal choice we ran a couple of models with 4500 shells, and we see that the results are the same as for the models with 450 shells. We also reproduced the results of de Araujo & Opher (1994) with good agreement, for the models that have small pressure gradients. The shocks that appear are treated with the inclusion of the artificial viscosity of Richmeyer and Newmann (Richmeyer & Morton 1967).

In another article, to appear elsewhere (Miranda 1998), all the tests and details of the spherical Lagrangian hydrodynamic code used in the present article are given.

We begin the calculations at $z_{rec} = 1500$ ($T_{rec} = 4000K$), the beginning of the recombination era, and we follow the evolution of the cloud until its collapse. The initial density perturbation can be given in the form of a power law spectrum as considered, for example, by Gott & Rees (1975)

$$\delta_i = \frac{\delta\rho}{\rho} = \left(\frac{M}{M_o}\right)^{-1/3} (1 + z_{rec})^{-1}, \quad (1)$$

with M the mass of the cloud, M_o is the reference mass and z_{rec} is the redshift of the recombination. We use $\Omega_o = 0.1$ (baryonic density parameter) and $H = 100 km s^{-1} Mpc^{-1}$ (the Hubble constant).

It is worth noting that the above equation gives the rms density fluctuations as a function of the mass scale. This equation sets the initial density contrast in our top hat profile model.

In many studies, dealing with the evolution and collapse of primordial structures (some of them referred to above), it is not specified when (at what redshift) the calculations are started. It is also considered that the proto-structure, under study, is already detached from the rest of the Universe and, as a result, it is not taken into account the expansion of the Universe. The merit of de Araujo and Opher's (1988, 1989, 1994) works was to take into account all the necessary ingredients to study the evolution of density perturbations but, by other hand, they unrealistically fixed the density profile of the perturbations during all the time of the cloud evolution.

In order to follow the evolution of density perturbations, it is necessary to start the calculations at the beginning of the recombination era, as mentioned above, including the expansion of the Universe and all the relevant processes that take place during and after the recombination era. Obviously, the results of the study will depend also on the density parameter, on the Hubble constant and on the density per-

turbation spectrum chosen as initial conditions. However, the three above ingredients are not completely known and thus, in the present article, we are considering different combinations of these three ingredients to follow the influence caused in the evolution of the clouds under study.

In §2 we describe the basic equations, in §3 we discuss our results and finally in §4 we present our conclusions.

2 BASIC EQUATIONS

The hydrodynamic equations that describe the dynamics of the primordial clouds are:

$$\frac{\partial\rho}{\partial t} + \frac{1}{r^2} \frac{\partial}{\partial r} (r^2 \rho v) = 0, \quad (2)$$

the mass conservation equation written in spherical coordinates; where ρ is the density of the cloud, r the radial coordinate and v the velocity. In our code the continuity equation is calculated directly from the grid. The specific volumes of the Lagrangian shells give the density of the cloud.

The equation of motion is given by:

$$\frac{D\vec{v}}{Dt} + \frac{1}{\rho} \nabla P + \nabla\phi + \frac{\sigma_T b T_r^4 x}{m_p c} \left[\vec{v} - \frac{\dot{R}(t)}{R(t)} \vec{r} \right] = 0 \quad (3)$$

where the velocity is $\vec{v} = \vec{v}_n + \vec{v}_H$ with \vec{v}_n the peculiar velocity of the cloud and $\vec{v}_H = H\vec{r}$ the Hubble flow; the pressure of the gas is $P = kN\rho T_m(1+x)$, with k the Boltzmann constant, N is the Avogadro's number, T_m is the temperature of the matter inside the cloud, and x the degree of ionization. The gravitational potential is ϕ , σ_T the Thomson cross section, $b = 4\sigma_{SB}/c$ (with σ_{SB} the Stefan-Boltzmann constant), T_r is the temperature of the radiation, m_p is the proton mass, c the velocity of light, $H(t) = \dot{R}(t)/R(t)$ with $R(t)$ the scale factor and $\dot{R}(t)$ its time derivative, and $D/Dt \equiv \partial_t + v\partial_r$ is the total derivative.

The energy equation is written as:

$$\frac{DE}{Dt} = \frac{P}{\rho^2} \frac{D\rho}{Dt} - L \quad (4)$$

where E is the thermal energy per gram and L the cooling function.

The cooling-heating processes are included in the cooling function L which is given by the summation of four mechanisms:

$$L = L_R + L_C + L_{H_2} + L_\alpha \quad (5)$$

The heat conduction is not taken into account due to the fact that the clouds, that we are studying, never reach temperatures in which heat conduction is important. Bremsstrahlung was also not included because the temperatures of the matter inside the clouds never reach values above of $10^4 K$.

The cooling from recombination, L_R (see e.g. Schwarz et al 1972), is given by:

$$L_R = -kNT_m \frac{Dx}{Dt} = -kNT_m C \left\{ \beta e^{-(B_1-B_2)/kT_r} (1-x) - \frac{a\rho x^2}{m_p} \right\} + I, \quad (6)$$

where the constants $B_1, B_2, C, \beta, \Lambda_{2s,1s}$ are defined below. The function I (see Eq. 17) is the collisional ionization (see, e.g., Defouw 1970). Also, the term L_R takes into account the photoionization and the ionization due to collisions.

The Compton cooling-heating L_C is given by (see, e.g., Peebles 1968):

$$L_C = \frac{4kN\sigma_T b T_r^4 x}{m_e c} (T_m - T_r). \quad (7)$$

At high redshifts the Compton cooling-heating provides an important mechanism of energy exchange between the CBR and the electrons.

For the cooling by molecular hydrogen, L_{H_2} , we follow Lepp & Shull (1983), who give the following equations:

$$L_{H_2} = \frac{\Lambda}{\rho} \quad (\text{erg g}^{-1} \text{s}^{-1}) \quad (8)$$

The electronic ground state of these molecules may be excited to rotational and vibrational levels as a result of collisions with atomic hydrogen, emitting infrared photons and hence cooling the cloud. We use the equations given by Lepp & Shull (1983) where they represent a good fit for $100K \leq T_m \leq 10^5 K$.

The equation to determine Λ is given by:

$$\Lambda = n_{H_2} \left[\frac{L_{RH}}{1 + \frac{L_{RH}}{L_{RL}}} + \frac{L_{VH}}{1 + \frac{L_{VH}}{L_{VL}}} \right] \quad (9)$$

with:

$$(i) L_{VH} = 1.1 \times 10^{-18} e^{-(6744/T_m)};$$

$$(ii) L_{VL} = 8.18 \times 10^{-25} n_H T_m^{1/2} e^{-(1000/T_m)} \quad (\text{for } T_m \geq 1635K)$$

or

$$L_{VL} = 11.45 \times 10^{-26} n_H e^{[(T_m/125) - (T_m/577)^2]} \quad (\text{for } T_m < 1635K);$$

$$(iii) L_{RH} = 3.9 \times 10^{-19} e^{-(6118/T_m)} \quad (\text{for } T_m \geq 1087K)$$

or

$$L_{RH} = 10^{(-19.24 + 0.47y - 1.247y^2)} \quad (\text{for } T_m < 1087K);$$

$$(iv) L_{RL} = (n_{H_2}^{0.77} + 1.2n_H^{0.77}) \times 1.38 \times 10^{-22} e^{-(9234/T_m)} \quad (\text{for } T_m \geq 4031K)$$

or

$$L_{RL} = (n_{H_2}^{0.77} + 1.2n_H^{0.77}) \times 10^{(-22.9 - 0.553y - 1.148y^2)} \quad (\text{for } T_m < 4031K).$$

In the above equations n_{H_2} is the numerical density of H_2 , n_H is the numerical density of H and $y = \log(T_r/10^4)$.

The reactions which produce H_2 , used in our calculations, are shown below:

$$a) H + e \rightarrow H^- + h\nu \\ c_1 = 1.1 \times 10^{-18} T_m \text{ cm}^3 \text{s}^{-1} \text{ (H)}$$

$$b) H + H^- \rightarrow H_2 + e \\ c_2 = 2 \times 10^{-9} \text{ cm}^3 \text{s}^{-1} \text{ (BD)}$$

$$c) H^- + h\nu \rightarrow H + e$$

$$c_3 = 1.5 \times 10^{-2} T_r^{2.4} e^{-(8.75 \times 10^3/T_r)} \text{ s}^{-1} \text{ (MST)}$$

$$d) H^+ + H^- \rightarrow 2H + h\nu$$

$$c_4 = 1.7 \times 10^{-6} \times T_m^{-1/2} \text{ cm}^3 \text{s}^{-1} \text{ (PAMS)}$$

$$e) H^+ + H^- \rightarrow H_2^+ + e$$

$$c_5 = 5.6 \times 10^{-9} T_m^{-0.325} \text{ cm}^3 \text{s}^{-1} \text{ (PBCMw)}$$

$$f) H + H^+ \rightarrow H_2^+ + h\nu$$

$$c_6 = 3.4 \times 10^{-22} T_m^{3/2} \text{ cm}^3 \text{s}^{-1} \text{ (RP)}$$

$$g) H_2^+ + H \rightarrow H_2 + H^+$$

$$c_7 = 6.4 \times 10^{-10} \text{ cm}^3 \text{s}^{-1} \text{ (KAH)}$$

$$h) H_2^+ + h\nu \rightarrow H^+ + H$$

$$c_8 = 1.1 \times 10^{-13} T_r^{5.34} e^{-(10^4/T_r)} \text{ s}^{-1} \text{ (MST)}$$

$$i) H_2^+ + e \rightarrow 2H^+$$

$$c_9 = 1.35 \times 10^{-7} T_m^{-1/2} \text{ cm}^3 \text{s}^{-1} \text{ (GBD)}$$

$$j) H_2 + H \rightarrow 3H$$

$$c_{10} = \frac{k_H}{\left(\frac{k_H}{k_L}\right)^{[1/(1+n_H/n_{cr})]}} \text{ cm}^3 \text{s}^{-1} \text{ (LS)}$$

where c_i are the rates of production (or destruction) of the ions or molecules,

$$n_{cr} = 10^{(4-0.416s-0.327s^2)} \text{ cm}^3, s = \log(T_m/10^4),$$

$$k_H = 3.52 \times 10^{-9} e^{-(43900/T_m)} \text{ cm}^3 \text{s}^{-1},$$

$$k_L = 6.11 \times 10^{-14} e^{-(29300/T_m)} \text{ cm}^3 \text{s}^{-1} \text{ if } T_m \geq 7390K$$

or

$$k_L = 2.67 \times 10^{-15} e^{-(6750/T_m)^2} \text{ cm}^3 \text{s}^{-1} \text{ if } T_m < 7390K.$$

The references used for the above rates are: (H) – Hirasawa 1969, (BD) – Browne & Dalgarno 1969, (MST) – Matsuda, Sato & Takeda 1969, (PAMS) – Peterson, Abertz, Moseley & Sheridan 1971, (PBCMw) – Poulaert, Brouillard, Claeys, McGowan & Wassenhove 1978, (RP) – Ramaker & Peek 1976, (KAH) – Karpas, Anicich & Huntress 1979, (GBD) – Giusti-Suzor, Bardsley & Derkits 1983, (LS) – Lepp & Shull 1983.

Due to the fact that the clouds here studied are made of pure hydrogen, the above reactions are the most relevant to the formation and destruction of molecular hydrogen. Even if we included He, or even Li, in our studies, they would not contribute significantly to the cooling of the cloud, due to the temperatures and densities involved in our calculations.

The rates and production of ions and molecules are calculated by:

a) Molecular formation rate via H^-

$$x_{H^-} = \frac{n_{H^-}}{n_H} = \frac{x(1-x)nc_1}{n[(1-x)c_2 + x(c_4 + c_5)] + c_3} \quad (10)$$

$$\frac{dx_{H_2}}{dt} = (c_2 x_{H^-} - c_{10} x_{H_2}) n (1-x) \quad (11)$$

b) Molecular formation rate via H_2^+

$$x_{H_2^+} = \frac{n_{H_2^+}}{n_H} = \frac{nx[x_{H^-}c_5 - (1+x)c_6]}{n[(1-x)c_7 + xc_9] + c_8} \quad (12)$$

$$\frac{dx_{H_2}}{dt} = n(1-x)[c_7x_{H_2^+} - c_{10}x_{H_2}] \quad (13)$$

The Lyman- α cooling is (e.g., Calberg 1981) given by:

$$L_\alpha = 1.25 \times 10^{-11} C_{12} \frac{A_{2\gamma}}{A_{2\gamma} + C_{21}} \quad (erg/s) \quad (14)$$

where $A_{2\gamma} = 8.272 \text{ s}^{-1}$ is the two photon emission rate, $C_{21} = 1.2 \times 10^{-6} T_m^{-1/2} x n_H \text{ s}^{-1}$ the collisional de-excitation rate and $C_{12} = 2C_{21}e^{-(1.19 \times 10^5 / T_m)}$.

For the ionization degree we follow Peebles (1968) modified to take into account the collisional ionization. The ionization rate is then written as follows:

$$\frac{Dx}{Dt} = C \left\{ \beta e^{-(B_1 - B_2)/kT_r} (1 - x) - \frac{a\rho x^2}{m_p} \right\} + I \quad (15)$$

where B_1 , is the bound energy of the ground state and B_2 is the bound energy of the first excited state and:

$$C = \frac{\Lambda_{2s,1s}}{\Lambda_{2s,1s} + \beta}, \quad \beta = \frac{(2\pi m_e k T_r)^{3/2}}{h^3} e^{-(B_2/kT_r)} a \quad (16)$$

with $\Lambda_{2s,1s} = 8.227 \text{ s}^{-1}$ and $a = 2.84 \times 10^{-11} T_m^{-1/2} \text{ cm}^3 \text{ s}^{-1}$, the recombination rate.

The collisional ionization rate I (see e.g., Defouw 1970) is given by:

$$I = 1.23 \times 10^{-5} x n (1+x) \rho \frac{k}{B_1} T_m^{1/2} e^{-(B_1/kT_m)} \quad (17)$$

3 BOUNDARY CONDITIONS

The clouds evolve within a medium (the Universe) of density ρ_u and thus, we take into account the influence of the external medium on the evolution of the density perturbation. The expansion of the Universe is also considered because the physical parameters of the primordial clouds such as the density, the temperature and the degree of ionization depends on the Universe expansion rate. It is worth stressing that in many studies of structure formation the influence of the external medium on the structure under study was not taken into consideration.

In order to calculate the temperature of the matter of the Universe we consider, in the cooling function, only the contribution due to the Compton cooling-heating and the cooling due to the recombination processes. The other physical processes considered for the cloud are not relevant for the evolution of the matter temperature of the Universe.

The energy equation is then written as

$$\frac{dE_u}{dt} = \frac{P}{\rho_u^2} \frac{d\rho_u}{dt} - L_R - L_C. \quad (18)$$

For the degree of ionization of the Universe, we use directly the results of the study done by Peebles (1968), therefore without taking into account the collisional ionization, since it is not important for the matter evolution of the Universe. Thus, the degree of ionization is given by:

$$\frac{dx_u}{dt} = C \left\{ \beta e^{-(B_1 - B_2)/kT_r} (1 - x_u) - \frac{a\rho_u x_u^2}{m_p} \right\}, \quad (19)$$

$$C = \frac{\Lambda_{2s,1s}}{\Lambda_{2s,1s} + \beta}, \quad \beta = \frac{(2\pi m_e k T_r)^{3/2}}{h^3} e^{-(B_2/kT_r)} a \quad (20)$$

with $\Lambda_{2s,1s} = 8.227 \text{ s}^{-1}$ and $a = 2.84 \times 10^{-11} T_{mu}^{-1/2} \text{ cm}^3 \text{ s}^{-1}$.

4 CALCULATIONS AND DISCUSSIONS

The formation of objects in the Universe may be produced directly either from primordial density perturbations or through fragmentation or still agregation of objects that are also produced from primordial density perturbations.

We study here, in particular, the formation of the Population III objects ranging from $10M_\odot$ to $10^6 M_\odot$. In the present work we study the formation of these objects considering that they could be produced directly from a primordial density perturbation spectrum.

In many studies dealing with structure formation, it is considered that the proto-object is already detached from the rest of the Universe and as a result does not undergo the influence of the expansion of the Universe. These calculations do not take into account how a density perturbation becomes a coupled object, and the studies begin at a redshift where a couple of the physical processes are not important any more.

The structures that we observe today certainly depend on the kind of the density perturbations produced primordially, and also on the physical processes present during and after the recombination era that are very important in development of these density perturbations.

What we do here is to study one step before the kind of study considered elsewhere, we mean, to see how a density perturbation could become a proto-object. In so doing, we start our calculations from the recombination era, and take into account a series of physical processes present during and after the recombination era. The evolution of a given density perturbation depends also on, the kind of density perturbation spectrum and on the kind of cosmology considered (i.e., values of the Hubble constant and density parameters for baryonic and non-baryonic dark matter).

To see how the formation of proto-objects depend on the particular spectrum used we consider different kinds of spectra. Also, we consider different cosmologies, restricting, however, to those cosmologies without non-baryonic dark matter. In another article (Oliveira et al 1998, hereafter paper II) we study structure formation taking into account the presence of non-baryonic dark matter.

Still, to see how the physical processes contribute to the evolution of a given density perturbation, particularly those effects in general not considered by other authors, we performed some calculations with and without such effects (below we see in details which physical processes we are referring to).

Concerning the presentation of our results, we show, in particular, three points in the cloud: the centre (that is the first shell), the middle shell, and the last shell (that is the edge of the cloud) as a function of time. In order to analyze the radial behavior, we show five different times: t_i – time at the recombination era, $t_2 = (t_3 - t_i)/2$, $t_3 = (t_f - t_i)/2$, $t_4 = (t_f - t_3)/2$ and t_f – the time at the collapse of the core.

Also, as mentioned before, all the calculations were started at the beginning of the recombination era ($z_{rec} \sim 1500$). Due to the expansion of the Universe, even the clouds that are already Jeans unstable and eventually collapse, undergo, initially, an expansion phase before collapsing. It can be shown (see, e.g., Peebles 1993 and Coles & Lucchin 1995) that for a cloud which stops expanding, its mean density relative to the background is given by:

$$\left(\frac{\bar{\rho}_{cloud}}{\rho}\right) = \left(\frac{3\pi}{4}\right)^2 \simeq 5.6 \quad (21)$$

The above figure corresponds to:

$$\left(\frac{\delta\bar{\rho}}{\rho}\right) \simeq 4.6 \quad (22)$$

It is worth stressing that the above number is a lower limit since it depends only on the expansion rate of the Universe (in this particular case an Einstein – de Sitter Universe) and on the gravity of the cloud. For the cases in which other physical processes are important the clouds stop expanding for

$$\left(\frac{\delta\bar{\rho}}{\rho}\right) > 4.6, \quad (23)$$

far greater than the linear regime. In this way there could exist clouds, in the nonlinear regime, that neither collapse nor stop expanding (see also paper II).

In the work by de Araujo & Opher (1988,1989) it is defined the collapse redshift when the cloud radius has 1/100 of the turn around radius (when the velocity $v = 0$, i.e., when the cloud stop expanding). In our calculation we consider that the cloud collapses when $\delta\rho/\rho \geq 10^4$. It is worth stressing that what we call a collapse it is, in fact, a condition for which the collapse of a proto-object become irreversible.

Let us have a look at the models for a Universe with $\Omega = 0.1$ and $h = 1.0$ (the Hubble constant in unit of $100 \text{ km s}^{-1} \text{ Mpc}^{-1}$), and let us consider a density perturbation given by Eq.(1) with $M_o = 10^{15} M_\odot$.

Let us first have a look at the evolution of the density contrast (Fig.1) that gives us information about the collapse of the clouds. Generally speaking, we see that there is no collapse for $M < 10^4 M_\odot$.

As expected, for $10 M_\odot$ the density contrast (as seen in Fig.1) falls rapidly in all shells and almost completely disappears when $z \sim 1250$. For $M = 10^2 M_\odot$ the same happens when $z \sim 1300$. For lower redshifts the density contrast oscillates for both masses. These results are expected, because at the time of the recombination era, these clouds were not Jeans unstable. Still, they tend to oscillate, but due to photon-drag the perturbations are strongly dissipated.

For the masses $10^3 M_\odot$ and $10^4 M_\odot$ the fate is a little bit different. In these cases the perturbations oscillate for

different shells, as can be seen, for instance, in the intermediate and internal shells of $M = 10^3 M_\odot$. For the external shells the perturbation decreases almost without oscillation. For the mass $10^4 M_\odot$ the behavior is similar to that of $M = 10^3 M_\odot$. Again, due to the fact that these clouds are not Jeans unstable at the time of the recombination era, the perturbations are strongly dissipated by the photon-drag. It is also worth noting that the cooling mechanisms are not efficient enough to cool down the clouds and turn them Jeans unstable.

The masses $10^5 M_\odot$ and $10^6 M_\odot$ suffer partial collapse, i.e., the core collapses while the external shells oscillate. The internal shells of, for example, $M = 10^5 M_\odot$, initially oscillate but, due to the cooling mechanisms, this part of the cloud becomes Jeans unstable and then collapses.

It is worth stressing that we start all the calculations with a “top hat” density contrast profile. For the masses $10 M_\odot$ and $10^2 M_\odot$, the density contrast remains almost uniform as a function of the radial coordinate. For the masses $10^3 M_\odot$ and $10^4 M_\odot$ small oscillations occur along the radial coordinate. For the masses $10^5 M_\odot$ and $10^6 M_\odot$, the density contrast profile begins approximately uniform, but it does not remain so as time goes on. This behavior shows that the “top hat” profile is not maintained throughout the cloud evolution. A “top hat” profile is maintained only when forces proportional to the spherical coordinate appears. As soon as the pressure gradients begin to be important in the cloud evolution the “top hat” density profile is destroyed.

Alternatively in Fig.2 we illustrate the time evolution of the density of the cloud. We see, clearly the decrease in the density as time goes on for clouds with masses smaller than $10^4 M_\odot$ and the partial collapse underwent by the clouds with $10^5 M_\odot$ and $10^6 M_\odot$. We also show the morphological behavior of the density profile (see Fig.3) in order to see how it is modified as a function of time.

Concerning the velocity profile, it begins linear but it changes with time. It is worth stressing that a linear velocity profile is consistent with a “top hat” density profile and vice-versa. The masses $10 M_\odot$ to $10^4 M_\odot$, for example, oscillate accompanying the similar behavior of the density contrast. For the masses $10^5 M_\odot$ and $10^6 M_\odot$ the velocity decreases when the density contrast increases, as expected. We conclude that the linear profile of the velocity, that, e.g., de Araujo & Opher (1989) assumed, appears to be a good approximation for the masses $10 M_\odot$ to $10^4 M_\odot$. But for the masses $10^5 M_\odot$ and $10^6 M_\odot$ the approximation is not valid. The internal pressure and the physical processes work to destroy the velocity linear profile, as a result the density profile is not a “top hat” like any more.

In the study of the collapse, the thermal and chemical history of the clouds are worth studying due to the fact that the evolution of the clouds in what concern, for example, their fragmentation depends on how the temperature of the clouds evolve which, by other hand, depend on their chemical ingredients. For primordial clouds, in particular, the thermal history will also depend on the Compton cooling (heating) processes, that maintains the temperature of the cloud close to the temperature the CBR. This cooling processes is particularly relevant for high values of z (i.e., $z > 300$).

As we explained above the heat conduction and the Bremsstrahlung is not taken into account. It is worth stress-

ing that in our study we do not take, as initial condition, a virialized object as considered by some authors. Our calculations start at the recombination era when the temperature of the matter inside the perturbation has the same value of that of the radiation. For clouds that collapse at high redshifts, in general, the principal mechanism that acts in the evolution and collapse of the perturbations is the Compton heating-cooling (see results presented in Tables 5-8). Thus, during the expansion phase of the perturbations, when the Compton heating-cooling is efficient, the temperature of the matter inside the perturbation is almost the same temperature of the radiation.

At the redshift collapse of the clouds, the temperature of the matter increases by a factor 4 or 5 in relation to its correspondent value at the turn-around. Thus the temperature of the clouds that collapse, due to shocks and the collapse itself, can rise to $\sim 10^4 K$ depending on the power spectrum and on the mass of the cloud (see, e.g. Table 2). Also, depending on the power spectrum and on the mass of the cloud, the shocks and the collapse itself are not able to rise the temperature of the cloud to $\sim 10^4 K$ (see, e.g., Table 3 and paper II).

Certainly, these results are dependent on the particular way in which we defined the collapse of the clouds. That is, we consider that an object collapsed when the density contrast is greater than 10^4 . The results also depend on the thermal history of the clouds (that depends on the physical processes here considered). As a result no strong shocks occur that could eventually heat the clouds to temperatures $> 10^4 K$. If we follow the calculations to higher values of density than the established by our collapse criterion, the temperature will rise above the values here obtained. It is possible that to density contrasts higher than 10^5 strong shocks occur and they would probably heat the gas to values of the order of the virial temperature, as a result other physical processes, as e.g. Bremsstrahlung, would be important to the evolution of the clouds.

Let us examine the temperature, pressure and molecular density formation of the clouds studied. The temperature, pressure and molecular density fall with time for the masses ranging from $10M_\odot$ to 10^4M_\odot , as seen in Fig.4. These are, in fact, expected results since the density perturbations are disappearing as time goes on. As a result, the cloud temperature, for example, tends to be equal to the temperature of the matter of the Universe.

For clouds with masses ranging from 10^5M_\odot to 10^6M_\odot , the behavior is very different. The pressure, for example, grows, since the cloud begins to collapse. The temperature initially decreases, but as time goes on it increases, but not significantly, which is so due to the fact that the cooling mechanisms become important and cool the cloud. During the collapse process there is an efficient formation of molecular hydrogen. The molecular hydrogen, and also the Compton cooling process are the most important cooling mechanisms for primordial clouds. It is worth mentioning that the Compton cooling (heating) process is important for high redshift (i.e. $z > 300$) as above mentioned, while the molecular hydrogen cooling is important for $z < 300$, which is so due to the fact that the CBR photoionize the H^- and H_2^+ ions that intermediate the formation of molecular hydrogen.

An analysis of the molecular density versus temperature of the cloud is shown in Fig.5. For the cloud of 10^6M_\odot ,

for example, the molecular density increases when the temperature is in the interval $100K < T < 500K$, which occurs during the cloud collapse. The molecular hydrogen is very important in the cooling processes of the cloud, as already mentioned.

For the masses $10M_\odot$ to 10^4M_\odot the pressure profile remains constant with time along the radial coordinate; only tiny variations are seen for the mass 10^4M_\odot . For other masses, the profile changes rapidly with time along the radial coordinate. The production of the molecules, and the consequent cooling of the cloud, is always more important in the central part of the cloud.

In Fig.6 we show how the radii of the shells of the clouds change with time. For the masses 10^5M_\odot and 10^6M_\odot , for example, we clearly see how the different shells of the clouds evolve with time. It is also possible to see that these clouds undergo a partial collapse, the outer most shells do not stop expanding.

In Table 1 we present, in particular, in its second and third column, a comparison between our results and the results of de Araujo (1990) for $M_o = 10^{15}M_\odot$. There we observe, e.g., that the mass 10^6M_\odot has collapse redshift similar to that obtained by de Araujo (1990). The mass 10^4M_\odot , however, collapses at $z_c = 5.4$ in the models of de Araujo (1990) but here there is no collapse for such a mass. The mass 10^5M_\odot collapses at $z_c = 260$ according to de Araujo (1990), but we obtained a collapse at $z_c = 22$. For clouds with masses larger than 10^6M_\odot the collapse redshift is almost the same, for these cases the pressure is not very important in the evolution of the cloud, this explain why the results are the same (see also paper II). For those cases in which the internal pressure is important on the evolution of the cloud the results are too different. In conclusion, it is not a good assumption to maintain a “top hat” density profile for clouds with masses less than 10^6M_\odot , as de Araujo (1990) considered throughout their calculations.

As mentioned earlier the clouds stop expanding satisfying Eq.(23), therefore well above the linear regime. Again we see in Table 1 in particular for a cloud of 10^6M_\odot that the present results agree with those by de Araujo (1990). For clouds in which the pressure is important the turn around occurs for values above the value given by Eq.(23). In the paper II we discuss this issue for clouds with masses larger than 10^6M_\odot , where we also include the presence of non-baryonic dark matter.

Another interesting comparison has to do with the minimum mass that can collapse in our model. We have found that the minimum mass is $\simeq 8.5 \times 10^4M_\odot$ (the collapse redshift is 12), that is almost one order of magnitude larger than that found by de Araujo (1990). This shows again that to fix the density profile is not a good assumption.

We obtained also a mass limit that does not collapse but remain bounded, namely, $3.8 \times 10^4M_\odot$. This bounded cloud reaches a density contrast of 10^4 , but the collapse does not evolve to a denser stage, it oscillates until the present time. In Fig.7 we see the behavior of the radii of the shells as a function of time for this mass.

It is worth stressing that these results just discussed are for a Universe model with $h = 1$ and $\Omega = 0.1$, with a reference mass $M_o = 10^{15}M_\odot$.

Obviously the results presented here depend on the particular spectrum of perturbations used. The minimum mass,

Table 1. The redshifts of collapse.

M/M_\odot	z_c	z_c^A	z_c^*	δ_{ta}^A	δ_{ta}
10^4	NC	5.4	NC	8.0	–
4.4×10^4	–	–	40	–	–
8.5×10^4	12	–	498	–	6.3
10^5	22	260	477	6.7	5.7
10^6	197	180	643	5.1	5.0

The redshifts of collapse of the present paper, z_c , and de Araujo's studies (de Araujo 1990), z_c^A , for $M_o = 10^{15} M_\odot$; and redshifts of collapse of the present paper for $M_o = 4 \times 10^{17} M_\odot$, z_c^* . The density contrast at the turn around for de Araujo's studies, δ_{ta}^A , and for the present paper, δ_{ta} , for $M_o = 10^{15} M_\odot$. NC stands for “no collapse”.

for example, that collapses would be different if we used a different spectrum of density perturbations. In Table 1 we also include the collapse redshift for the spectrum normalized with a reference mass $M_o = 4 \times 10^{17} M_\odot$ (instead of $10^{15} M_\odot$). The density perturbations with $M_o = 4 \times 10^{17} M_\odot$ are seven times greater than those with $M_o = 10^{15} M_\odot$. We may see that the collapse redshifts are altered significantly, and also the minimum mass that collapses is now $4.4 \times 10^4 M_\odot$ with a collapse redshift of ~ 40 (see Table 2).

Due to the fact that the collapses occur at a higher redshift for a large M_o , there is also a modification in the importance of the physical processes in the evolution of the clouds. The molecular hydrogen cooling, for example, is less significant for collapses which occur at high redshift.

When we change the content of baryonic matter from $\Omega = 0.1$ to $\Omega = 0.2$ and maintain $h = 1$ and $M_o = 10^{15} M_\odot$ the minimum mass becomes $5 \times 10^4 M_\odot$; the collapse occurring at $z=9$ (see Table 3). In Table 3 we show the collapse redshifts for clouds of different masses.

For $h = 0.5$, $\Omega = 0.1$ and $M_o = 10^{15} M_\odot$ we obtain that $2 \times 10^5 M_\odot$ is the minimum mass that collapses. The collapse occurs at $z=0.78$ (see Table 4).

The above results show that the minimum mass does not depend strongly neither on the kind of spectra used nor on the values of the Hubble constant and the density parameter assumed. By other hand, the collapse redshifts depend strongly on the Universe model and on the spectra adopted.

As we have already mentioned, the present study includes a series of physical processes not in general considered in the literature, namely, the Compton cooling (heating), the photon-drag due to the cosmic background radiation are examples.

We thus studied the influence of the cooling-heating processes and the photon-drag on the evolution of the clouds here considered. We chose, in particular, for this study, the clouds of 3.8×10^4 , 8.5×10^4 , 10^5 and $10^6 M_\odot$, the results are presented in Tables 5-8 respectively. To do this we studied individually the effects of all the four cooling-heating processes and the photon drag. The values in these tables have been taken for z_c , that is, the redshift when the collapse occurs.

First let us analyze the cooling from recombination. For the mass $3.8 \times 10^4 M_\odot$ we again do not have collapse when we disregard this cooling mechanism; for $8.5 \times 10^4 M_\odot$ the collapse is delayed. The collapse redshift changes from $z \sim$

Table 2. Values of the variables when we used $h = 1.0$, $\Omega = 0.1$ and $M_o = 4 \times 10^{17} M_\odot$.

M/M_\odot	z_c	$n_{H_2} (cm^{-3})$	$T (K)$	$\rho (g cm^{-3})$
10^4	NC	–	–	–
4.4×10^4	40	3×10^{-2}	7×10^3	8×10^{-19}
10^5	48	3×10^{-2}	7×10^3	8×10^{-19}
10^6	624	2×10^{-2}	7×10^3	5×10^{-17}

Table 3. Values of the variables when we used $h = 1.0$, $\Omega = 0.2$ and $M_o = 10^{15} M_\odot$.

M/M_\odot	z_c	$n_{H_2} (cm^{-3})$	$T (K)$	$\rho (g cm^{-3})$
5×10^4	9	300	100	3×10^{-22}
8.5×10^4	90	100	500	3×10^{-19}
10^5	123	320	500	1×10^{-18}
10^6	207	500	10^3	3×10^{-18}

Table 4. Values of the variables when we used $h = 0.5$, $\Omega = 0.1$ and $M_o = 10^{15} M_\odot$.

M/M_\odot	z_c	$n_{H_2} (cm^{-3})$	$T (K)$	$\rho (g cm^{-3})$
8.5×10^4	NC	2×10^{-12}	10	3×10^{-31}
10^5	NC	3×10^{-13}	10	3×10^{-31}
2×10^5	0.8	3×10^{-6}	50	3×10^{-25}
10^6	158	63	320	2×10^{-19}

12 with all processes to $z \sim 6.8$ without the recombination cooling. For the masses $10^5 M_\odot$ and $10^6 M_\odot$ this cooling does not affect the collapse redshift.

The Compton cooling-heating works against the collapse for the masses from $3.8 \times 10^4 M_\odot$ to $10^5 M_\odot$. When a cloud (density perturbation) begins to evolve, at the beginning of the recombination era, it first expands and then stop expanding if it becomes Jeans unstable, as already mentioned. During the expansion phase it would cool down adiabatically if we did not have any cooling-heating processes. In this way, the cloud could stop expanding and collapses earlier. Due to the Compton heating the cloud is heated to temperatures near to that of the cosmic background radiation, as a result the cloud stop expanding and collapses later.

Also, disregarding the Compton heating a cloud of $3.8 \times 10^4 M_\odot$ collapses. This means that the minimum mass depends on this very processes. For masses with $M < 10^6 M_\odot$ the collapse occurs earlier as we may see in Tables 5-8. For clouds with $M > 10^6 M_\odot$, however, the collapse redshift is not affected, again due to the fact that the pressure for this cloud does not significantly affect the collapse, because these clouds become Jeans unstable just after the recombination era.

In Fig.8 we present the time evolution of the temperature, pressure and molecular hydrogen density, with all physical processes included and without the Compton cooling-heating processes. It is seen that the evolution of the above physical quantities are very different, even for the case in which the redshift collapse is not significantly altered, namely, for clouds of $10^6 M_\odot$. In conclusion, the thermal history of the clouds studied is strongly dependent on the Compton heating process.

Table 5. Values of the variables for $M = 3.8 \times 10^4 M_\odot$ with $h = 1.0$, $\Omega = 0.1$ and $M_o = 10^{15} M_\odot$.

Variable	with all processes	without L_R	without L_C	without L_{H_2}	without L_α	without photon drag
z_c	NC	NC	156	NC	NC	NC
$n_{H_2} (cm^{-3})$	10^{-8}	10^{-8}	10^2	–	10^{-8}	10^{-10}
$T (K)$	50	50	10^2	50	50	50
$\rho (g cm^{-3})$	3×10^{-27}	3×10^{-27}	3×10^{-19}	2×10^{-27}	3×10^{-27}	1×10^{-30}

Table 6 Values of the variables for $M = 8.5 \times 10^4 M_\odot$ with $h = 1.0$, $\Omega = 0.1$ and $M_o = 10^{15} M_\odot$.

Variable	with all processes	without L_R	without L_C	without L_{H_2}	without L_α	without photon drag
z_c	12	6.8	252	2.7	6.8	2
$n_{H_2} (cm^{-3})$	10^{-2}	10^{-2}	3×10^{-2}	–	10^{-2}	3×10^{-4}
$T (K)$	10^2	10^2	7×10^3	4×10^2	10^2	10^2
$\rho (g cm^{-3})$	1×10^{-22}	1×10^{-22}	6×10^{-20}	1×10^{-23}	1×10^{-22}	3×10^{-24}

Table 7. Values of the variables for $M = 10^5 M_\odot$ with $h = 1.0$, $\Omega = 0.1$ and $M_o = 10^{15} M_\odot$.

Variable	with all processes	without L_R	without L_C	without L_{H_2}	without L_α	without photon drag
z_c	24	24	220	5	24	13
$n_{H_2} (cm^{-3})$	0.3	0.5	10^2	–	0.3	6×10^{-2}
$T (K)$	200	200	2×10^3	200	200	10^2
$\rho (g cm^{-3})$	3×10^{-21}	3×10^{-21}	2×10^{-18}	3×10^{-21}	3×10^{-21}	6×10^{-22}

Table 8 Values of the variables for $M = 10^6 M_\odot$ with $h = 1.0$, $\Omega = 0.1$ and $M_o = 10^{15} M_\odot$.

Variable	with all processes	without L_R	without L_C	without L_{H_2}	without L_α	without photon drag
z_c	194	194	196	157	194	246
$n_{H_2} (cm^{-3})$	800	800	800	–	10^2	10^2
$T (K)$	800	800	10^3	8×10^3	10^3	1300
$\rho (g cm^{-3})$	2×10^{-18}	2×10^{-18}	2×10^{-18}	1×10^{-18}	2×10^{-18}	3×10^{-18}

If we disregard the cooling by molecular hydrogen, the mass $3.8 \times 10^4 M_\odot$ is not significantly affected, there is no collapse in this case, as already seen there is no collapse even considering the molecular hydrogen cooling. The collapse for the other masses occur for lower values of redshift. Without such an important cooling process the pressure is greater and as a result there is a delay in the collapse of the cloud. In Fig.9 we can see the different behavior of the temperature, pressure and molecular density when this cooling is disregarded.

For the Lyman- α cooling the behavior of the collapse is similar to the cooling due to the recombination.

If we disregard the photon-drag process we observed that the collapse is delayed for masses $8.5 \times 10^4 M_\odot$ and $10^5 M_\odot$ and the collapse occurs earlier for the mass $10^6 M_\odot$.

The photon drag works like a brake for the expansion and for the collapse. If we have masses around the Jeans mass the behavior of these masses near the epoch of the collapse is strongly influenced by the photon drag.

When we disregard the photon drag for masses smaller

than $10^6 M_\odot$ the collapse is delayed, due to the fact that the cloud stop expanding later, beginning as a result to collapse later. This occurs, also because these clouds have $M \leq M_J$ (the Jeans mass).

If we have masses larger than $10^6 M_\odot$ (Jeans unstable masses) when we disconsider the photon drag, the cloud stop expanding earlier, and due to the fact that the pressure is not so important for these cases, the cloud collapses in a $t \sim t_{ff}$ (free-fall time). As a result the collapses occur earlier, without such an effect.

As a general conclusion we see that the cooling-heating processes are less effective for the mass $10^6 M_\odot$, in particular, concerning the epoch of the collapse, due to the fact that the pressure of the cloud in this case does not affect significantly its evolution. By other hand, the thermal history of the cloud, as well as, the amount of molecular hydrogen produced depend significantly on the physical processes here considered.

An important point concerning the present study is that we take into account the appropriate physics and begin the

calculations in the appropriate era, i.e., at the recombination era. These facts strongly influence the evolution of the clouds as we have shown above.

5 CONCLUSIONS

In the present work we studied the evolution of density perturbations with masses within the range $10 - 10^6 M_\odot$ taking into account a series of physical processes which are present during and after the recombination era. In order to perform such a study a spherical Lagrangian hydrodynamical code was written, with which it was possible to follow the spatial and time evolution of the density perturbations.

Our main conclusions are:

- a) For clouds with $M < 10^4 M_\odot$, no collapse occurs. In this case, the density perturbations are strongly dissipated by the photon-drag. Only a residual density perturbation remains; this conclusion holds for the two density perturbations spectra and for the different combinations of h and Ω adopted;
- b) Clouds of 10^5 and $10^6 M_\odot$ present a partial collapse;
- c) The minimal mass which collapses does not change significantly when we alter h , Ω and M_0 , namely, $M_{min} \sim 10^4 - 10^5 M_\odot$;
- d) When we disregard, for example, the Compton cooling-heating, the collapse for masses $> 8.5 \times 10^4 M_\odot$ occurs earlier;
- e) The photon-drag is a very important process, the collapse redshift, for example, is changed significantly when we disregard it, but it works differently for higher or smaller masses. For the smaller masses the photon-drag dissipates their density perturbations and for the higher masses it causes a delay in the collapse of the clouds.

ACKNOWLEDGEMENTS

The calculations were performed on a HP-Apollo 9000 (purchased by the Brazilian agency FAPESP) and on the CRAY computers EL98 and J90 (CCE/USP).

We would like to thank Dr David Weinberg, the referee, for his helpful suggestions and comments that greatly improved the present version of our paper. We would also like to thank the Brazilian agencies CAPES (SRO) and CNPq (ODM, JCNA and RO) for financial support.

REFERENCES

- Browne J.C., Dalgarno A., 1969, J. Phys, 2, 885
 Calberg R.G., 1981, MNRAS, 197, 1021
 Cen R., 1992, ApJ, 78, 341
 Coles P., Lucchin F., 1995, Cosmology. The Origin and Evolution of Cosmic Structure, John Wiley & Sons, New York
 de Araujo J.C.N., 1990, PhD thesis, AGA-120, IAG-USP
 de Araujo J.C.N., Opher R., 1988, MNRAS, 231, 923
 de Araujo J.C.N., Opher R., 1989, MNRAS, 239, 371
 de Araujo J.C.N., Opher R., 1994, ApJ, 437, 556
 Defouw R.J., 1970, ApJ, 161, 55
 Giusti-Suzor A., Bardsley J.N., Derkits C., 1983, Phys. Rev. A, 28, 682
 Gott III R., Rees M.J., 1975, A&A, 45, 365
 Haiman Z., Thoul A.A., Loeb A., 1996, ApJ, 464, 523
 Hirasawa T., 1969, Prog. Theor. Phys., 42, 523

- Hutchins J.B., 1976, ApJ, 205, 103
 Karpas Z., Anicich V., Huntress W.T., 1979, J. Chem. Phys., 70, 2877
 Lepp S., Shull J.M., 1983, ApJ, 270, 578
 Matsuda T., Sato H., Takeda H., 1969, Prog. Theor. Phys., 42, 219
 Miranda O.D., 1998, in preparation
 Oliveira S.R., Miranda O.D., de Araujo J.C.N., Opher R., 1998, MNRAS (submitted) - Paper II
 Palla F., Salpeter E., Stahler S., 1983, ApJ, 271, 632
 Peebles P.J.E., 1968, ApJ, 153, 1
 Peebles P.J.E., 1993, Principles of Physical Cosmology, Princeton UP, Princeton
 Peterson J.R., Abertz W.H., Moseley J.T., Sheridan J.R. 1971, Phys. Rev. A, 3, 1651
 Poulaert G., Brouillard F., Claeys W., McGowat J. W., Wassenhove G. van, 1978, J. Phys. B, 11, 21
 Ramaker D., Peek J., 1976, Phys. Rev. A, 13, 58
 Richtmeyer R.D., Morton K.W., 1967, Difference Methods for Initial Value Problems, Interscience Pub., New York
 Schwartz J., MacCray R., Stein R.F., 1972, ApJ, 175, 673
 Thoul A.A., Weinberg D., 1995, ApJ, 442, 480

FIGURE CAPTIONS

Fig.1 – The evolution of the density contrast (δ) with time. The solid line is the internal shell, the short dashed line is the middle shell and the long dashed line is the external shell. Time is in years (the input parameters are $M_o = 10^{15} M_\odot$, $h = 1.0$, $\Omega = 0.1$).

Fig.2 – The evolution of the mass density ρ ($g\ cm^{-3}$) with time. The captions and input parameters for the curves are the same as in Fig.1.

Fig.3 – The mass density versus the radial coordinate (in pc) of the cloud. The solid line is the initial time (t_i), the short dashed line, long dashed line and very long dashed line are intermediate times (respectively t_2 , t_3 and t_4). The dashed-pointed line is the final time (t_f). The input parameters are the same as in Fig.1.

Fig.4 – The evolution of the temperature (T in K), pressure (P in $dyn\ cm^{-2}$) and density of molecules (n_{H_2} in $molecules\ cm^{-3}$) with time. The captions and input parameters for the curves are the same as in Fig.1.

Fig.5 – The evolution of the density of molecules (n_{H_2}) versus temperature. The captions and input parameters for the curves are the same as in Fig.1.

Fig.6 – The evolution of the radial coordinate of the clouds with time. The captions and input parameters for the curves are the same as in Fig.1.

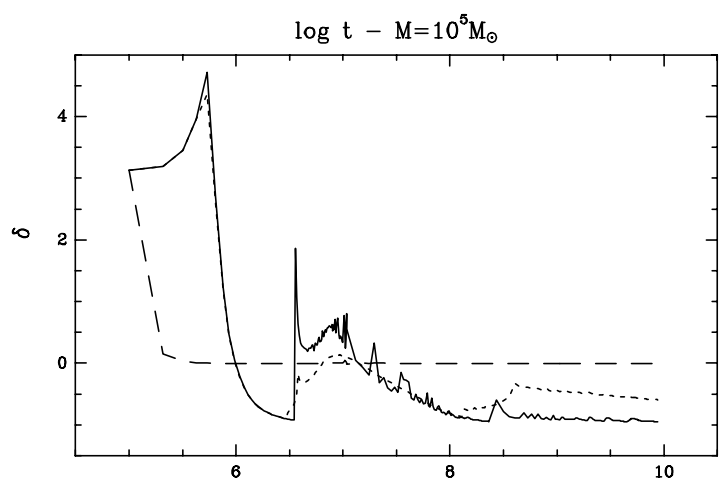
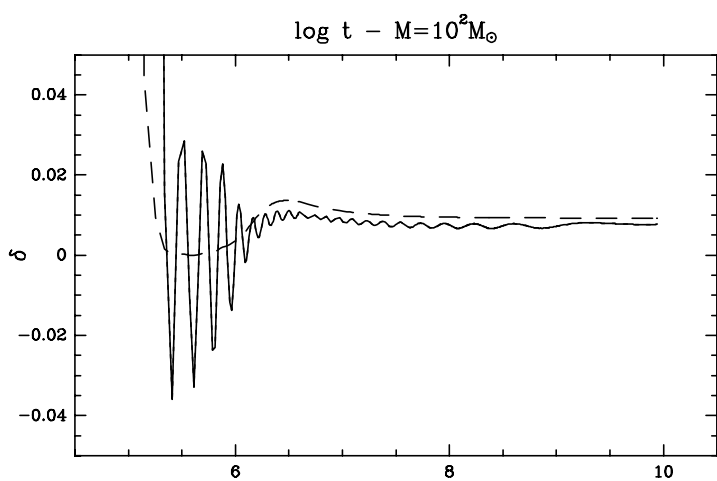
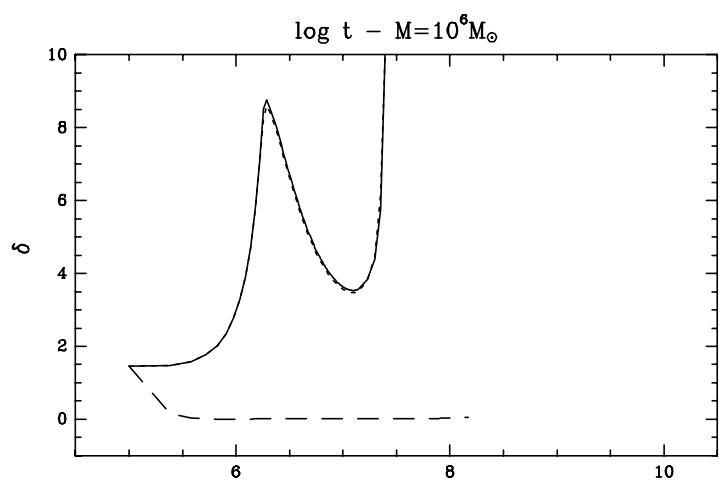
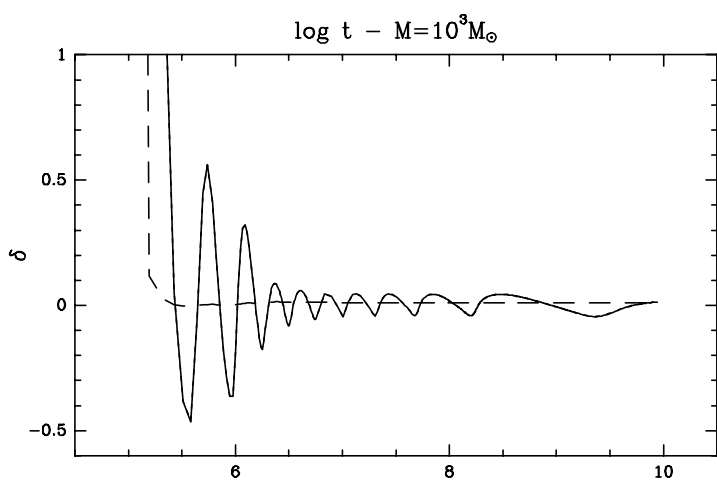
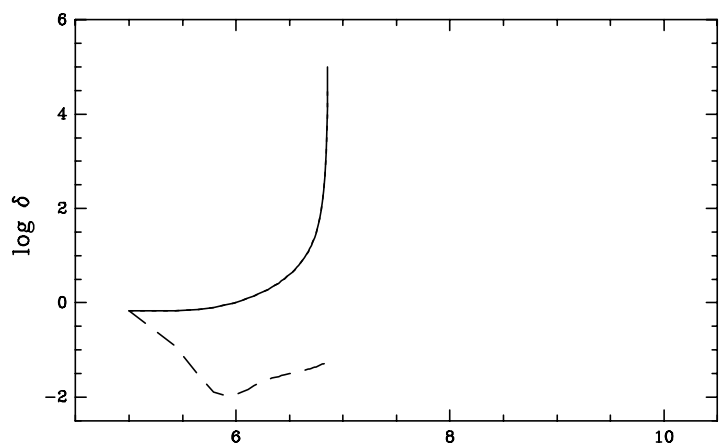
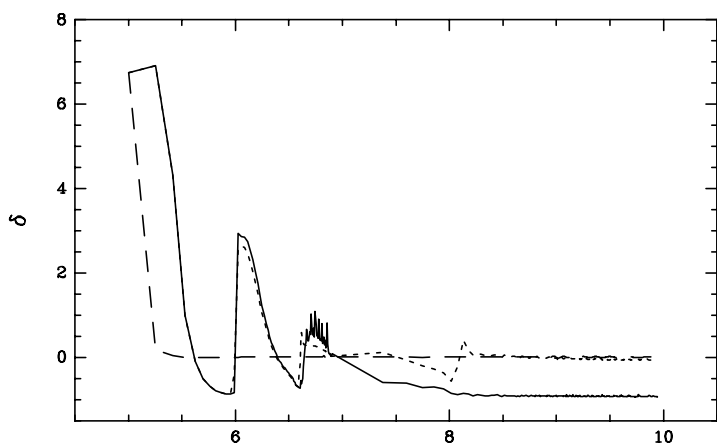
Fig.7 – The evolution of the radial coordinate of the mass $M = 3.8 \times 10^4 M_\odot$ with time. The captions and input parameters for the curves are the same as in Fig.1.

Fig.8 – The evolution of the temperature (T), pressure (P) and density of molecules (n_{H_2}) with time for masses $M = 3.8 \times 10^4 M_\odot$, $M = 8.5 \times 10^4 M_\odot$, $M = 10^5 M_\odot$ and $M = 10^6 M_\odot$ with all physical processes included and when we disregard the Compton cooling-heating. The captions and input parameters for the curves are the same as in Fig.1.

Fig.9 – The evolution of the temperature (T), pressure (P) and density of molecules (n_{H_2}) for masses $M = 3.8 \times$

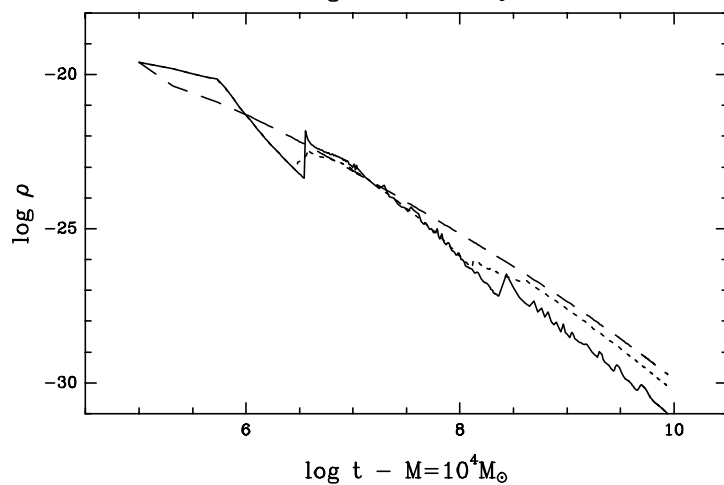
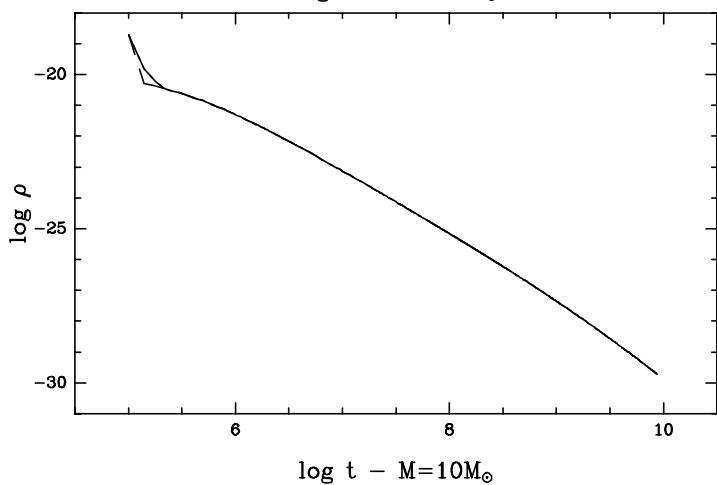
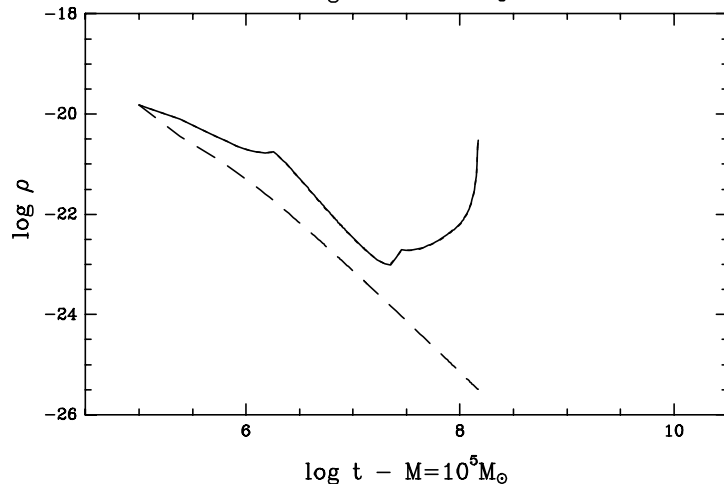
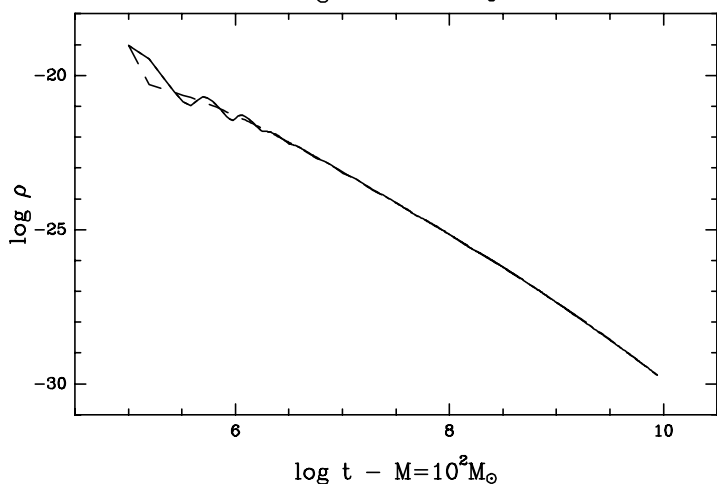
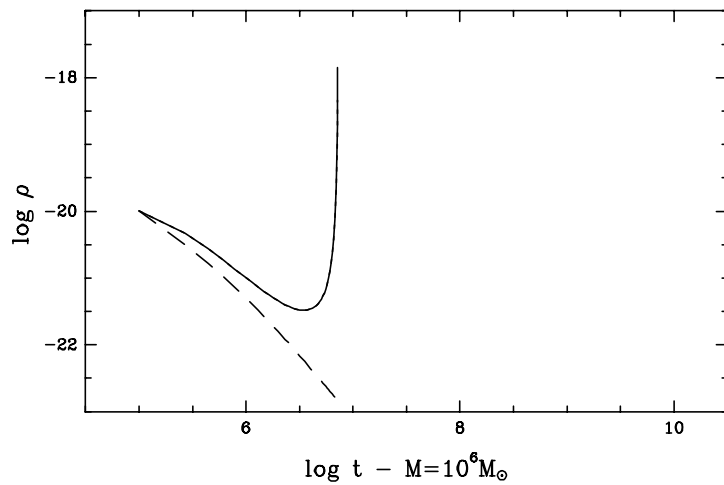
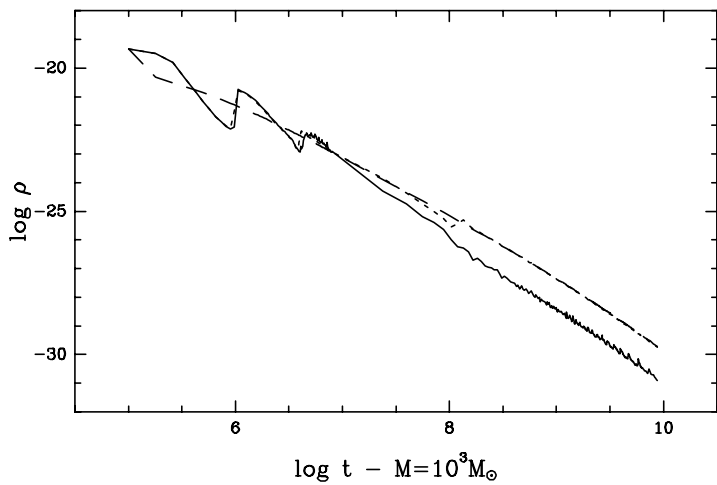
$10^4 M_\odot$, $M = 8.5 \times 10^4 M_\odot$, $M = 10^5 M_\odot$ and $M = 10^6 M_\odot$ with all physical processes included and when we disregard the H_2 cooling. The captions and input parameters for the curves are the same as in Fig.1.

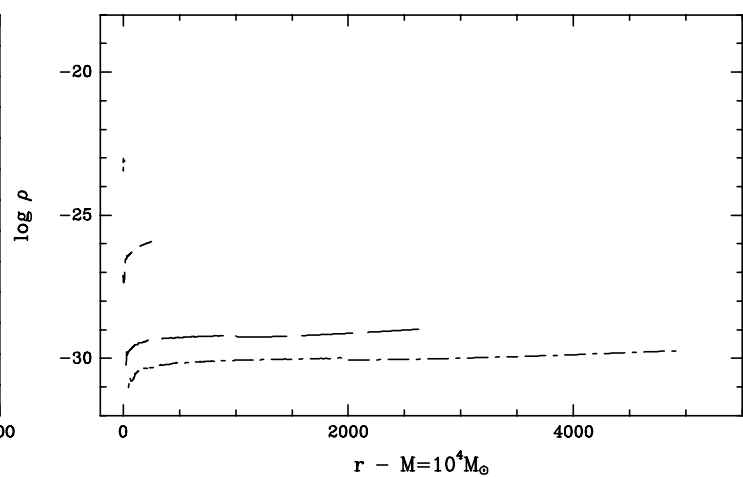
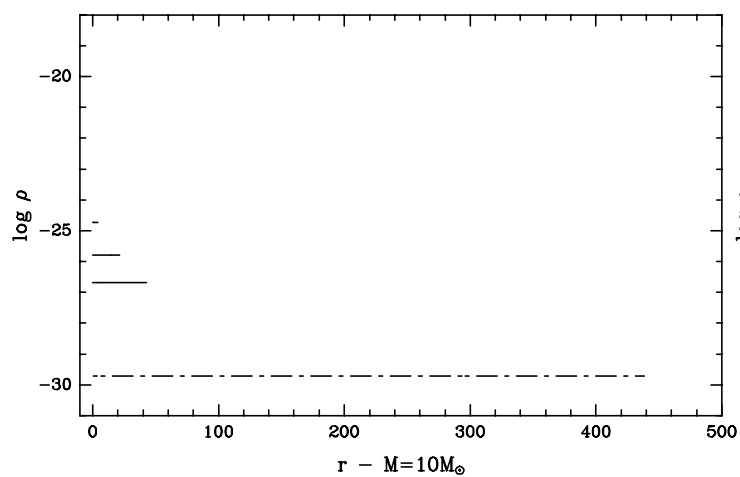
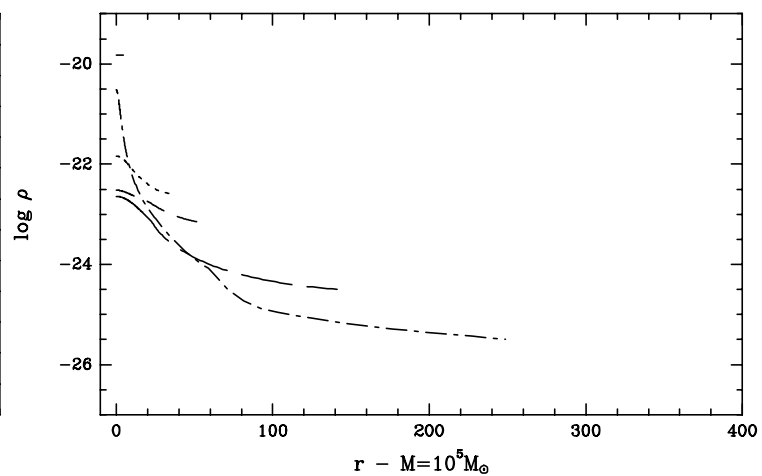
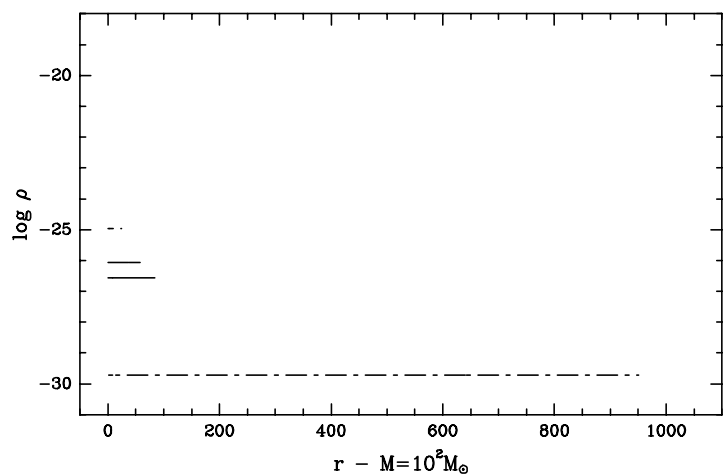
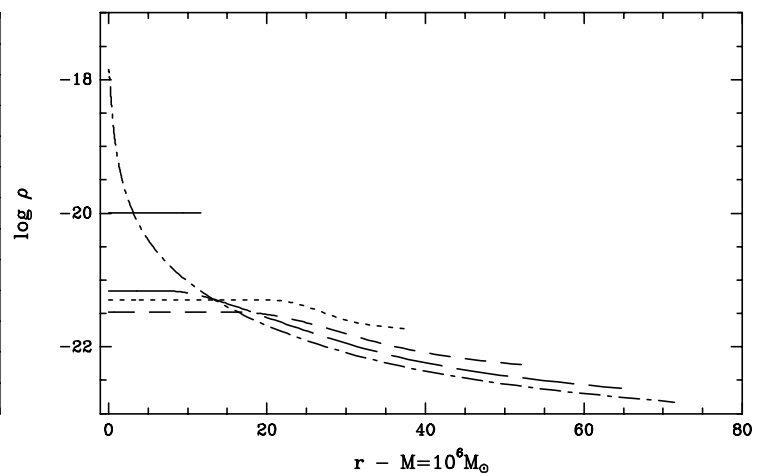
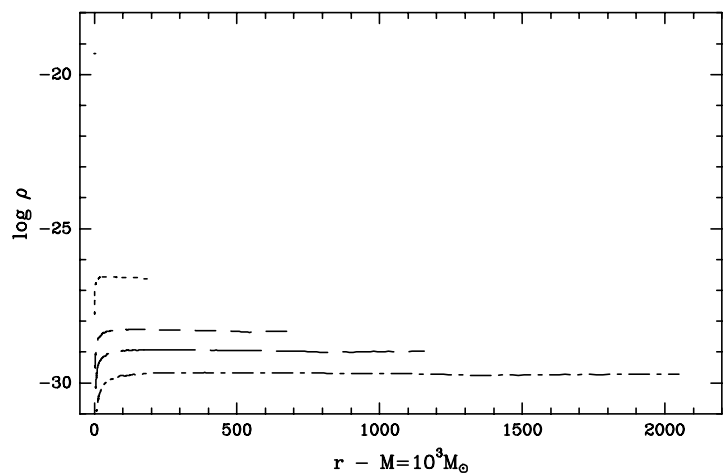
This paper has been produced using the Royal Astronomical Society/Blackwell Science \LaTeX macros.

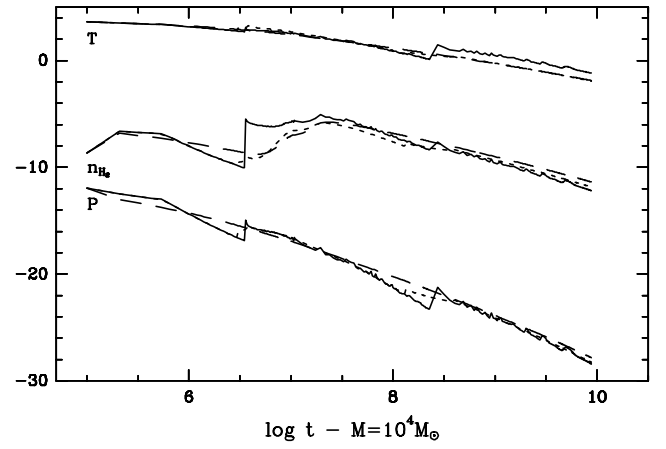
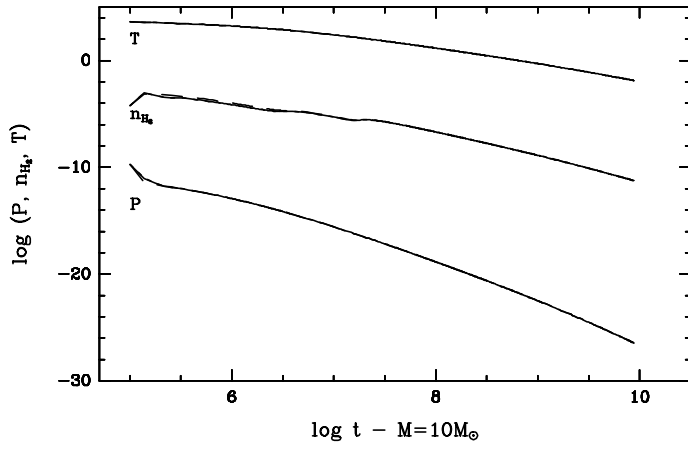
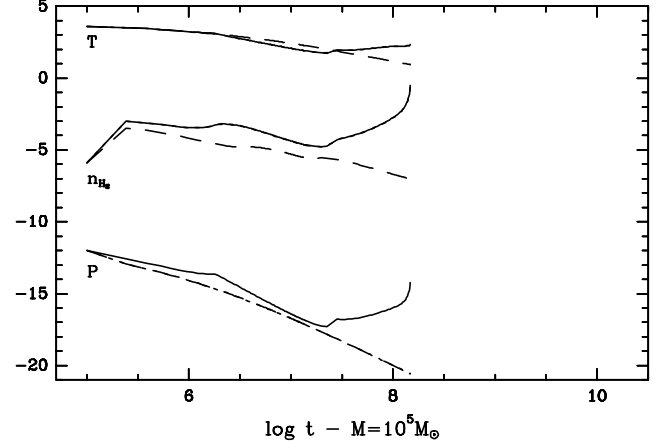
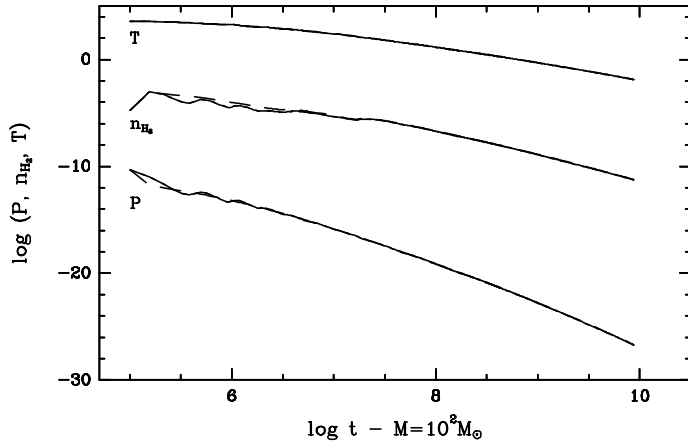
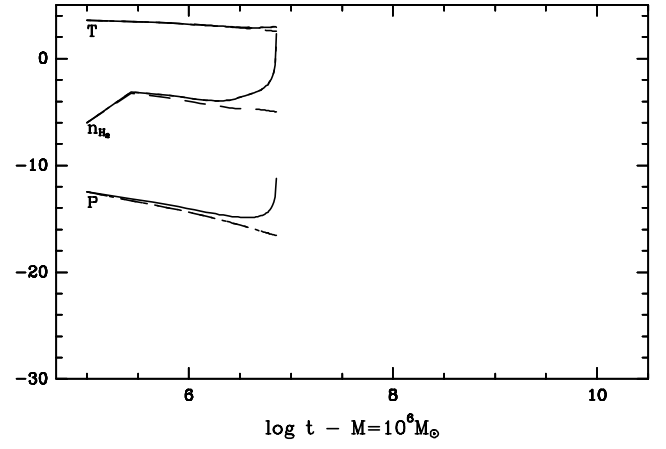
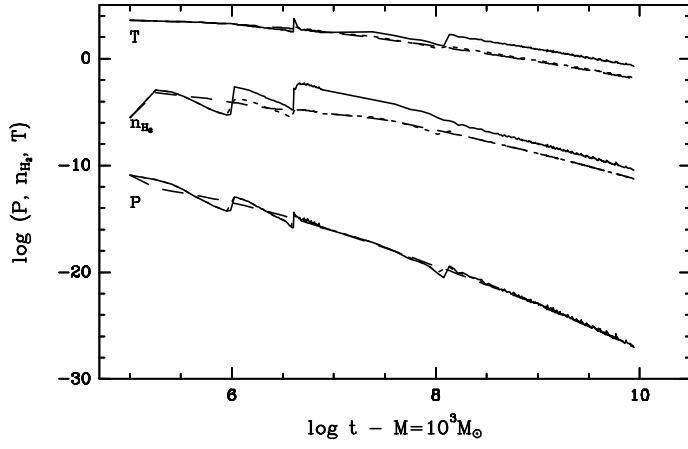


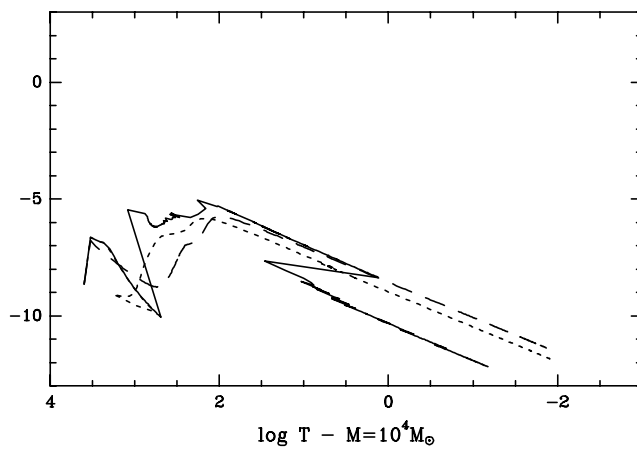
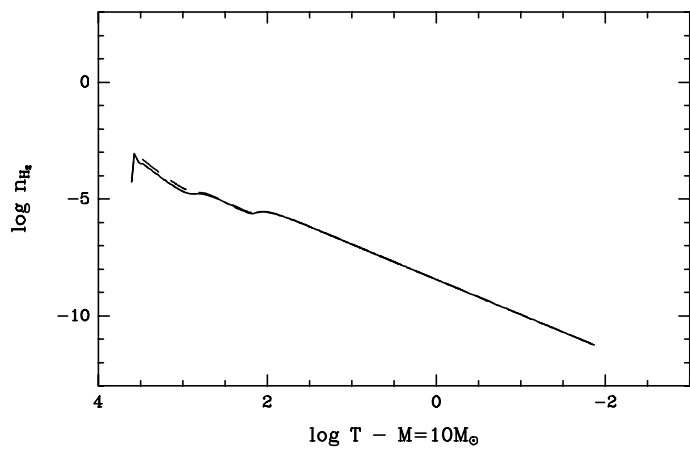
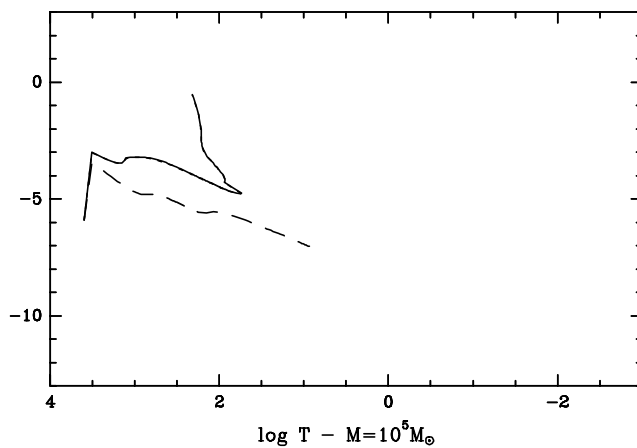
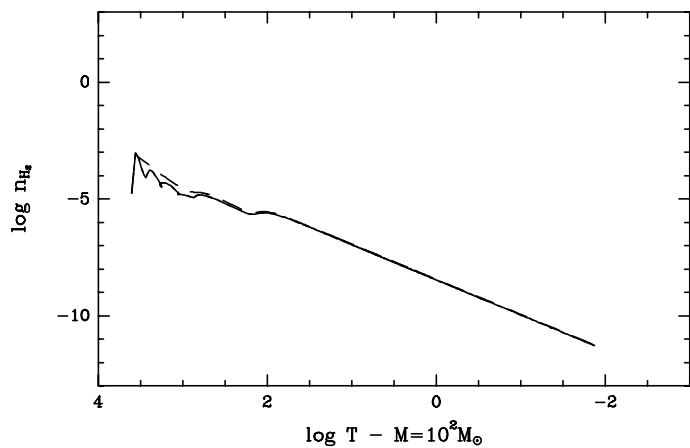
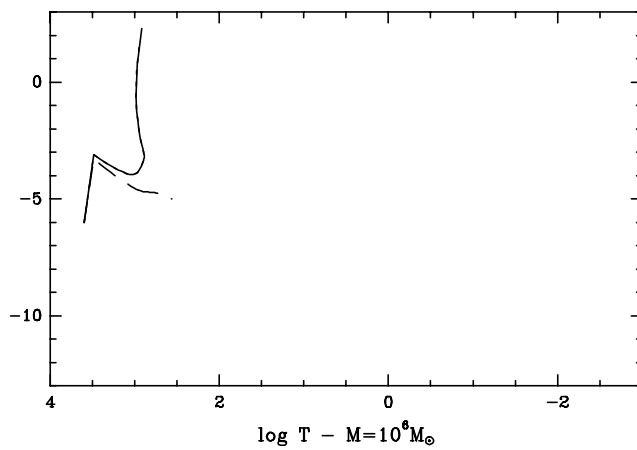
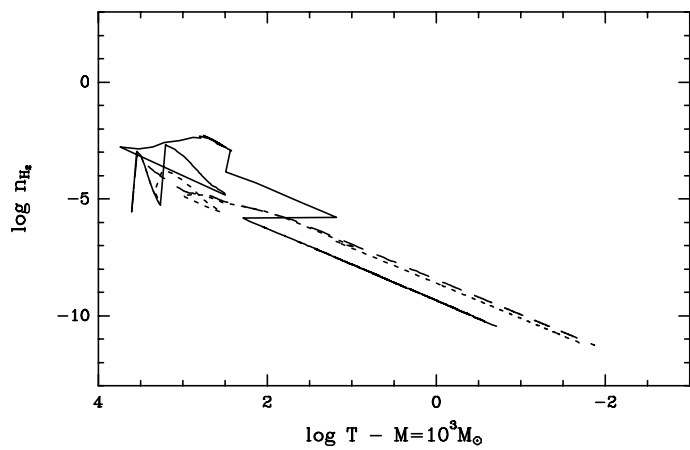
$\log t - M=10 M_\odot$

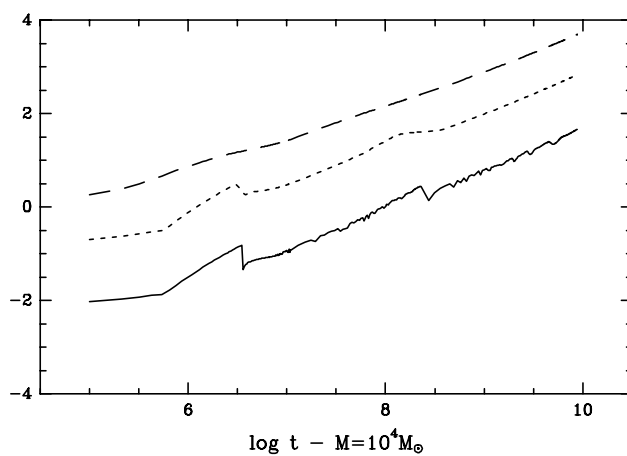
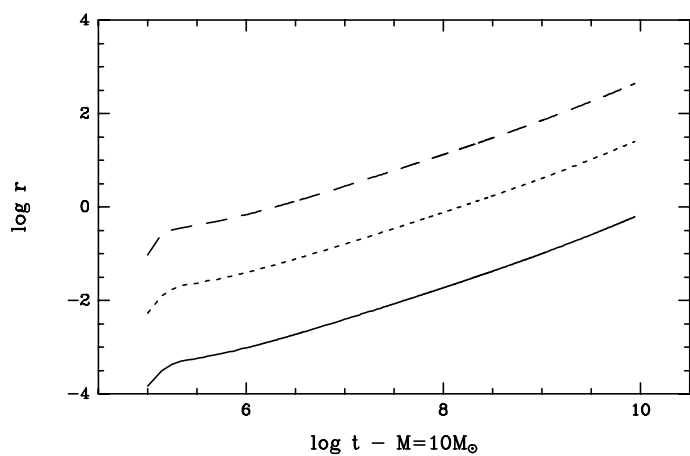
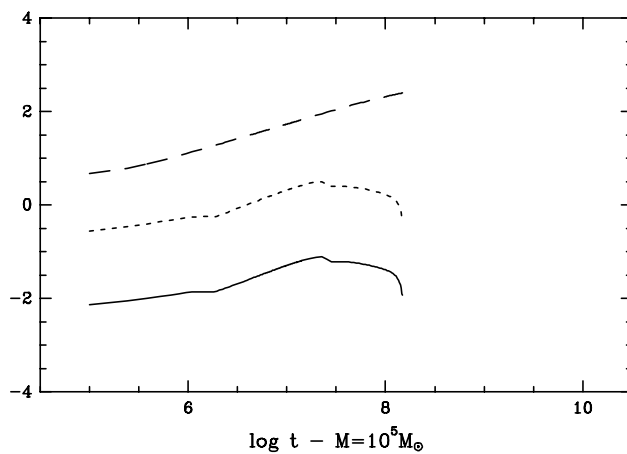
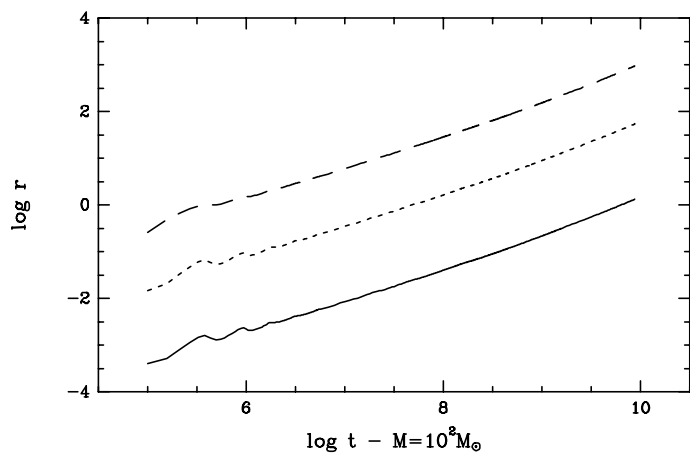
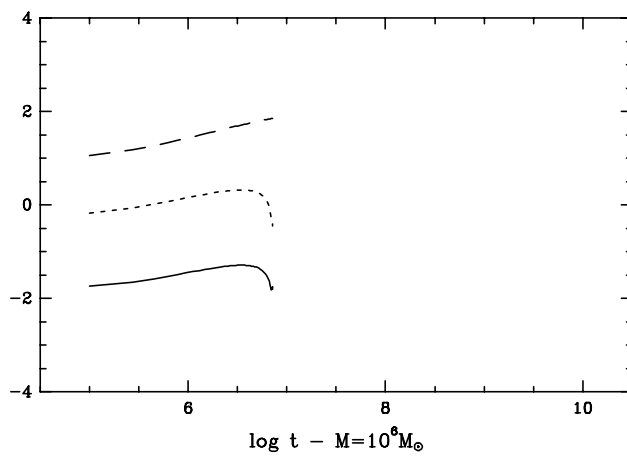
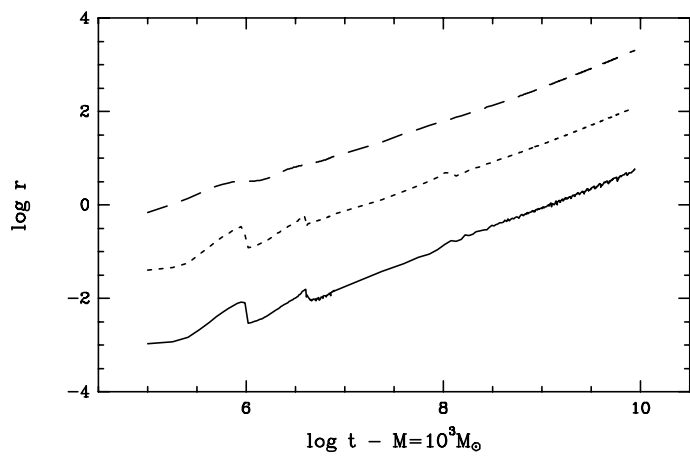
$\log t - M=10^4 M_\odot$

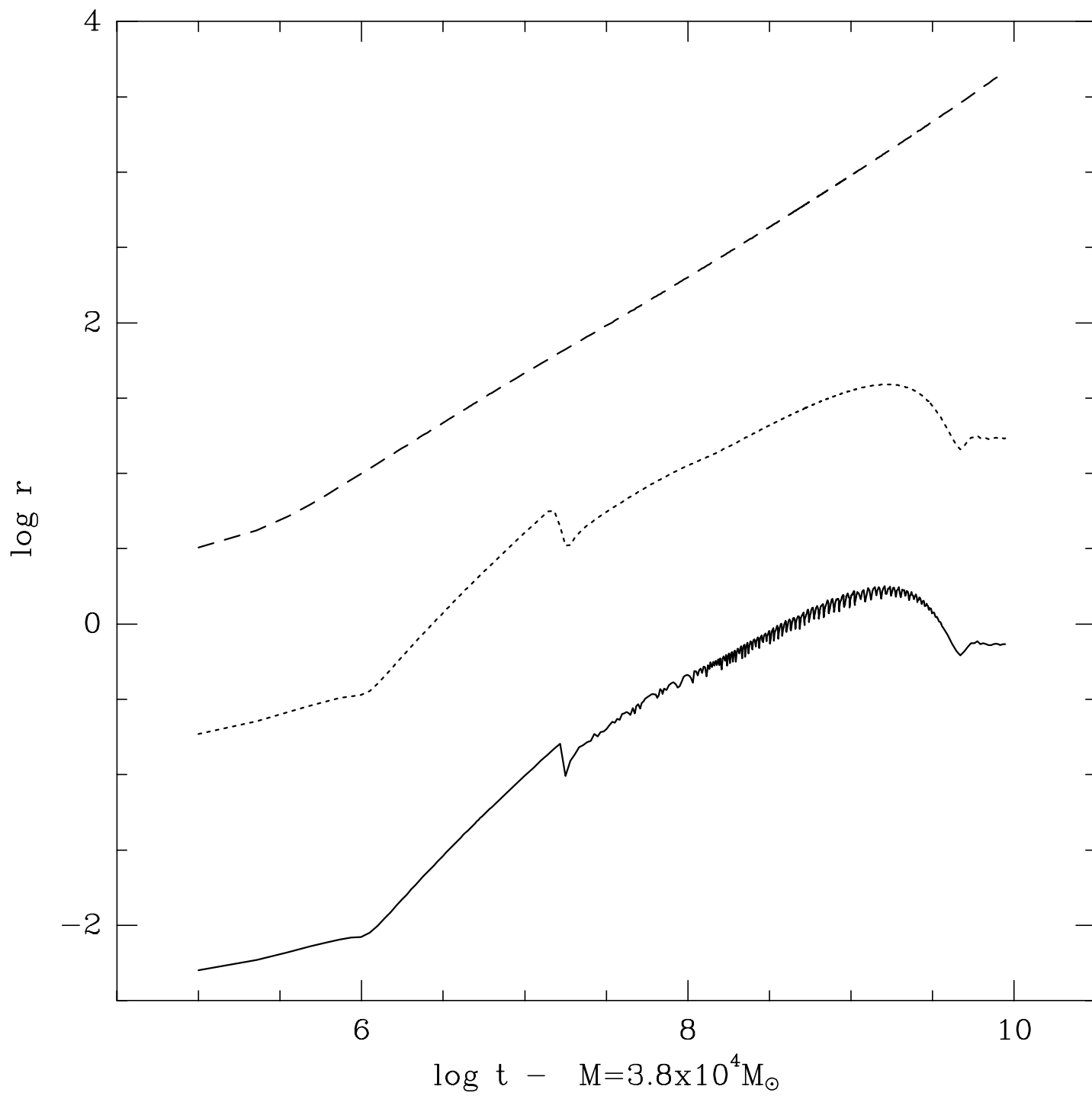


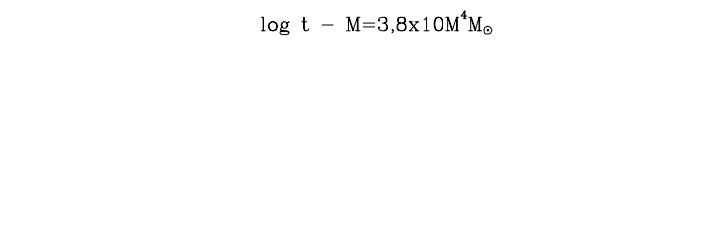
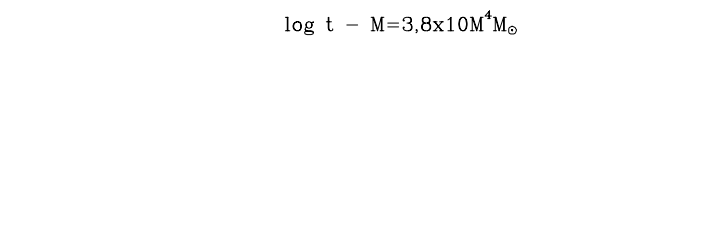
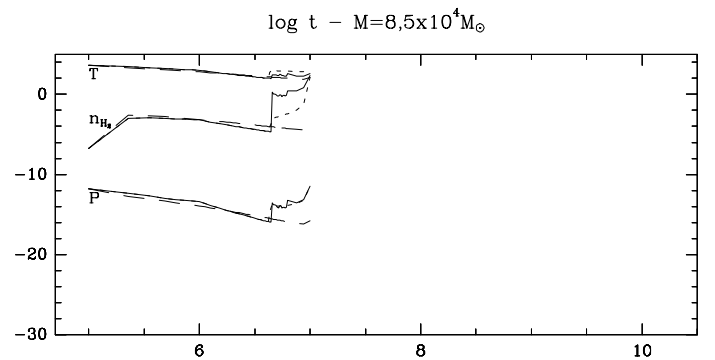
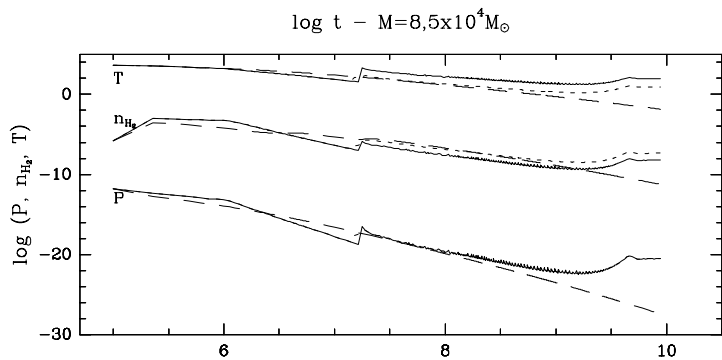
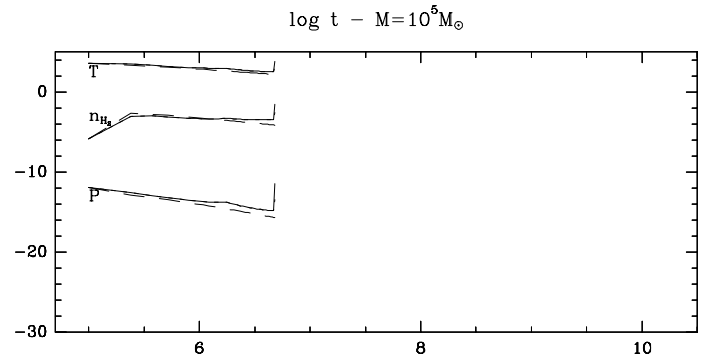
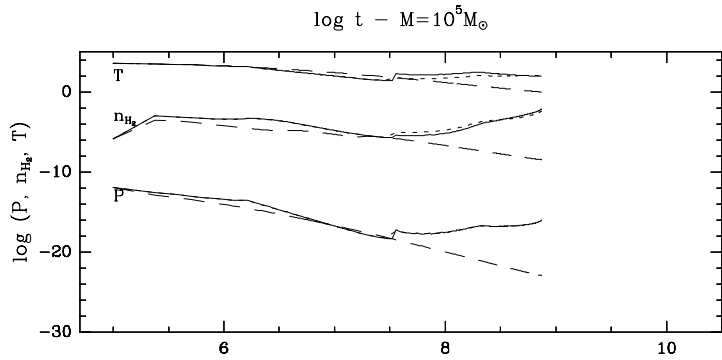
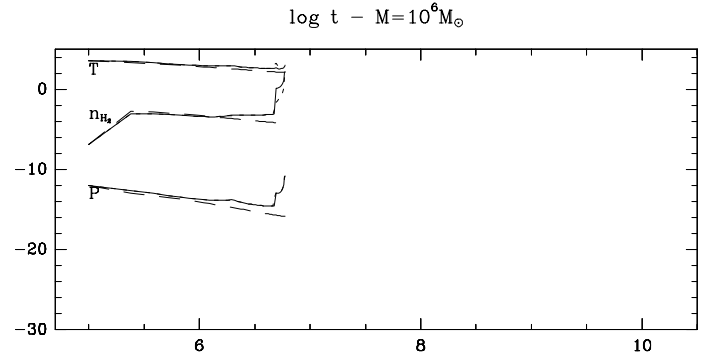
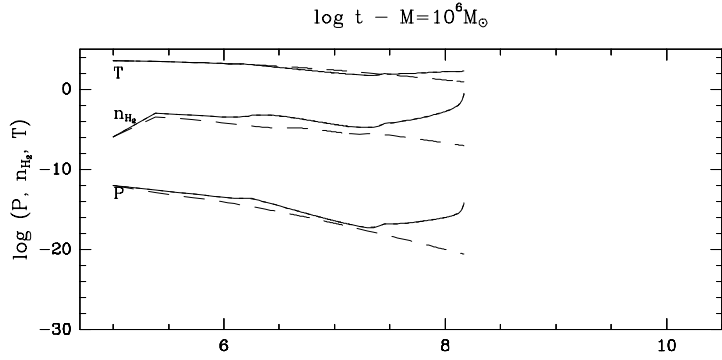
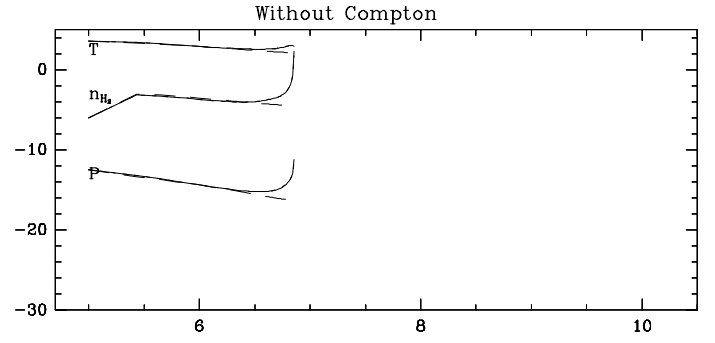
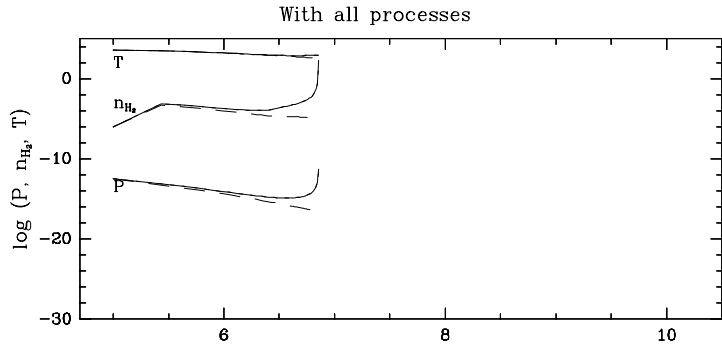




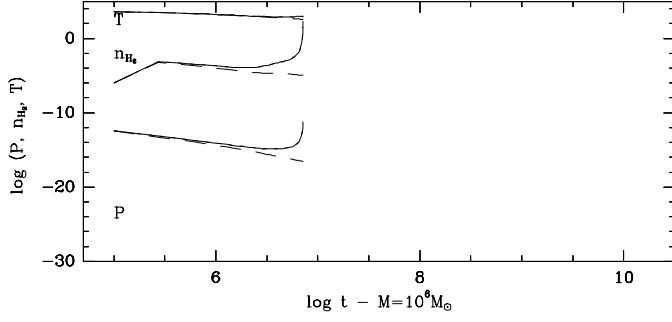








With all processes



Without molecules

